

# Spin Domains Generate Hierarchical Ground State Structure in $J = \pm 1$ Spin Glasses

Guy Hed<sup>1</sup>, Alexander K. Hartmann<sup>2</sup>, Dietrich Stauffer<sup>3</sup> and Eytan Domany<sup>1</sup>

<sup>1</sup> *Department of Physics of Complex Systems, Weizmann Institute of Science, Rehovot 76100, Israel*

<sup>2</sup> *Institut für Theoretische Physik, Universität Göttingen, Bunsenstr. 9, 37073 Göttingen, Germany*

<sup>3</sup> *Institute for Theoretical Physics, University of Cologne, Zùlpicher Straße 77, D-50937 Köln, Germany*

(December 2, 2024)

Unbiased samples of ground states were generated for the short-range Ising spin glass with  $J_{ij} = \pm 1$ , in three dimensions. Clustering the ground states revealed their hierarchical structure, which is explained by correlated spin domains, serving as cores for macroscopic zero energy “excitations”.

PACS numbers: 75.10.Nr, 75.50.Lk, 05.50+q, 75.40.Mg

Mean-field theory [1] provides a commonly accepted description of the low  $T$  phase of infinite-range spin glasses [2]. It predicts many pure states with a hierarchical ultrametric organization and a non-trivial state overlap distribution  $P(q)$ . Although this structure was suggested to hold also for short-range spin glasses (SRSG) [3], the equilibrium properties of these are still controversial. The main dispute concerns the number of different thermodynamic (pure) states of the system below  $T_c$ . Fisher and Huse [4] studied SRSG with continuously distributed couplings. According to them, a finite region embedded in an infinite system will be in one of two pure states. They describe the system’s low energy excitations above the local ground state as droplets - flipped spin domains of size  $L$  with surface tension  $\propto L^\theta$ . This structure, of two pure states dominating the low  $T$  phase yields, for any finite region of the infinite system, a trivial  $P(q)$  distribution. Numerical evidence for non-trivial  $P(q)$  in finite systems [5–7] does not contradict the droplet picture [8].

We present here evidence for a new picture of the spin glass phase. *It possesses some characteristics of the mean-field description, such as non-trivial  $P(q)$  and a hierarchical (non-ultrametric!) structure of the pure states; nevertheless, it is also consistent with the droplet picture.*

*The model:* We study the ground states (GS) of the Edwards-Anderson model [9] of an Ising spin glass

$$\mathcal{H} = \sum_{\langle ij \rangle} J_{ij} S_i S_j, \quad J_{ij} = \pm 1 \quad (1)$$

$\langle ij \rangle$  denotes nearest neighbor sites of a simple cubic lattice; the values  $J_{ij} = \pm 1$  are assigned to each bond independently and with equal probabilities [10]. Although this model is very special - it has highly degenerate GS [11] - we expect that its low- $T$  properties are generic, i.e. not qualitatively different from other  $\{J_{ij}\}$  distributions (such as Gaussian). On the other hand, the low- $T$  properties of (1) are most probably dominated by the structure of its GS. Hence we hope that the GS of the  $J = \pm 1$  model provide insight about the low- $T$  behavior of generic short-range Ising spin glass. In any case, the GS structure of this model is interesting on its own merit.

By combining very efficient algorithms [12] that produce ground states of this model, with simulated temper-

ing (ST) [13], we generated *unbiased* samples of the GS; i.e. we “equilibrated” our system at  $T = 0$ . We studied the model (1) with periodic boundary conditions in 3 dimensions, with  $N = L^3$  spins, for  $L = 4, 5, 6, 8$ . For each size  $L$  we produced 800 to 1000 realizations  $\{J\}$ ; for each realization an unbiased sample of  $M = 500$  GS has been generated and analyzed.

*Summary of the main results:* 1. For any given  $\{J\}$ , the GS do *not* cover the hypercube  $\mathbf{S} = (S_1, S_2, \dots, S_N)$  uniformly; rather, there is a *hierarchical structure*, as shown schematically in Fig. 1 and in detail in 2. The set of all GS splits into two clusters  $\mathcal{C}$  and  $\bar{\mathcal{C}}$ , related by *spin reversal*;  $\mathcal{C}$  splits into  $\mathcal{C}_1$  and  $\mathcal{C}_2$ , and so on.

2. This structure is generated by domains of highly correlated spins [14], with very different sizes. Separation of GS into  $\mathcal{C}$  and  $\bar{\mathcal{C}}$  is determined by the largest domain  $\mathcal{G}_1$ , whose size is typically larger than  $N/2$ . Two states in which  $\mathcal{G}_1$  has the same orientation have a much higher overlap than two states in which the spins of  $\mathcal{G}_1$  are inverted. This implies formation of two clusters of states,  $\mathcal{C}$  and  $\bar{\mathcal{C}}$ , corresponding to the two possible orientations of  $\mathcal{G}_1$ . The same structure persists at the next level, where the second largest cluster  $\mathcal{G}_2$  determines the partition of  $\mathcal{C}$  into  $\mathcal{C}_1$  and  $\mathcal{C}_2$  (see Fig. 1). Note that  $\mathcal{G}_1$  has the same orientation in these two clusters.

3. The hierarchical structure of the GS is due to large differences between the sizes of the spin domains (typically  $|\mathcal{G}_1| > 4|\mathcal{G}_2|$ ). For domains of equal sizes no hierarchy would have been observed.

4. This picture *differs* from mean-field; the correlated domains determine the overlap distribution, and the GS do not exhibit ultrametricity. On the other hand, if in the  $L \rightarrow \infty$  limit all but a vanishing fraction of the spins belong to compact [15] macroscopic correlated domains  $\mathcal{G}_a$ , then any finite region of the infinite system will exhibit a trivial  $P(q)$ , in agreement with the droplet picture.

We explain how this picture of GS structure and spin clusters has been found; we present evidence that substantiates our findings, investigate their dependence on system size and discuss their implications.

*Generating unbiased samples of ground states:* For every realization  $\{J_{ij}\}$  we used the *genetic cluster exact approximation* (CEA) algorithm [12] to sample the GS. Samples obtained by CEA are, however, biased [16], over

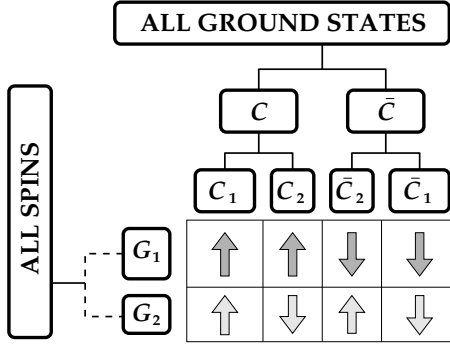


FIG. 1. Schematic representation of our picture; the two largest spin domains and the first two levels in the hierarchical organization of the GS are shown. The structure of the GS is explained by the spin domains' orientations; e.g. in the GS of the two sets  $\mathcal{C}_1, \mathcal{C}_2$ , the spins of  $\mathcal{G}_1$  have the same orientation, whereas the spins of the smaller cluster,  $\mathcal{G}_2$ , have flipped.

weighting GS from small *valleys* (a valley  $V$  consists of all the GS that can be traversed flipping one spin at a time) - therefore the probability to miss a valley is *lower* than that of an unbiased method. We used three methods to overcome this bias. For  $L = 4, 5$  and  $6$  we succeeded, for most realizations  $\{J\}$ , to enumerate exactly all GS within each valley; selecting at random  $M$  of the GS ensures that each valley is represented according to its size. For some  $\{J\}$  enumeration was not possible; then we used ST [13] to generate samples (our Glauber dynamics had a decorrelation time of less than two sampling periods for each spin). For  $L = 8$  we estimated the size of each valley by the method of [17] and generated a sample of GS in a valley by a Metropolis MC procedure. To test that this method [17] indeed yields unbiased GS, we sampled 60 realizations with ST, and ascertained that for the quantities of significance for our claims (the size of  $\mathcal{G}_2$  and the average correlation  $\bar{c}_{12}$  of the domains - see below) the estimates obtained by the two ways did not differ significantly and systematically.

*Clustering methodology:* Clustering is a powerful way to perform exploratory analysis of all kinds of data. In general, one calculates a *distance matrix*  $d_{ij}$  between the  $i = 1, \dots, n$  data points, and determines the underlying hierarchy of partitions (clusters) in the data. We used Ward's agglomerative algorithm [18]; it starts with each data point as a separate cluster and at each step fuses the pair of clusters  $\alpha, \beta$  that are at the shortest effective distance  $\rho_{\alpha\beta}$  from each other, stopping when all points are in one cluster. Initially  $\rho_{\alpha\beta} = d_{\alpha\beta}$ ; when two clusters  $\alpha, \beta$  are fused, the distances of the new cluster  $\alpha'$  to all unchanged clusters  $\gamma \neq \alpha, \beta$  are updated [18]:

$$\rho_{\alpha'\gamma} = \frac{(n_\alpha + n_\gamma)\rho_{\alpha\gamma} + (n_\beta + n_\gamma)\rho_{\beta\gamma} - n_\gamma\rho_{\alpha\beta}}{n_\alpha + n_\beta + n_\gamma} \quad (2)$$

where  $n_x$  is the number of points in cluster  $x$ . The algorithm produces a dendrogram such as Fig. 2(a). Leaves represent individual data points. The boxes at the nodes represent clusters; they are ordered horizontally in a way

that reflects their proximity. The vertical coordinate of cluster  $\alpha'$  is  $\tau(\alpha') = \rho_{\alpha\beta}$ , i.e. the effective distance between the two clusters that were fused to form  $\alpha'$ . For the initial (single state) clusters we set  $\tau = 0$ . When we fuse two "natural" clusters, whose separation exceeds significantly their linear extent, the branch *above* them is long. Hence we can identify "natural" sub-partitions of a cluster; as evident from Fig. 2(a),  $\mathcal{C}_1, \mathcal{C}_2$  are such natural sub-partitions of  $\mathcal{C}$ , and also  $\mathcal{C}, \bar{\mathcal{C}}$  are natural sub-clusters of the set of all GS. For each realization we analyzed the data in *two ways*: 1. viewing the GS as  $M$  data-points and 2. viewing the spins as  $N$  data-points.

*Clustering the Ground States:* Define the distance  $D_{\mu\nu} = (1 - q_{\mu\nu})/2$  between states  $\mathbf{S}^\mu$  and  $\mathbf{S}^\nu$ ;  $q_{\mu\nu} = \sum_i S_i^\mu S_i^\nu / N$  is their overlap. The dendrogram obtained by clustering 500 GS for a system with  $6^3$  spins is shown in Fig 2(a). Hierarchical GS structure is evident. To provide a quantitative measure of the extent to which a partition (of, say,  $\mathcal{C}$  to  $\mathcal{C}_1$  and  $\mathcal{C}_2$ ) is "natural", we evaluate the average distance *between* points in  $\mathcal{C}$  and  $\bar{\mathcal{C}}$ ,

$$D(\mathcal{C}, \bar{\mathcal{C}}) = \frac{1}{|\mathcal{C}||\bar{\mathcal{C}}|} \sum_{\mu \in \mathcal{C}} \sum_{\nu \in \bar{\mathcal{C}}} D_{\mu\nu} \quad (3)$$

and compare it to  $D(\mathcal{C})$ , the average distance *within*  $\mathcal{C}$ . In the same manner we define  $D(\mathcal{C}_1, \mathcal{C}_2)$ ,  $D(\mathcal{C}_1)$  and  $D(\mathcal{C}_2)$ . For  $L = 6$  we obtained  $D(\mathcal{C}) = 0.094(\text{mean}) \pm 0.067(\text{s.d.})$ ;  $D(\mathcal{C}, \bar{\mathcal{C}}) = 0.906 \pm 0.067$ ;  $D(\mathcal{C}_1) = 0.057 \pm 0.045$ ;  $D(\mathcal{C}_2) = 0.058 \pm 0.036$ ;  $D(\mathcal{C}_1, \mathcal{C}_2) = 0.178 \pm 0.143$ . For  $L = 8$  we obtained  $D(\mathcal{C}) = 0.078 \pm 0.050$ ;  $D(\mathcal{C}, \bar{\mathcal{C}}) = 0.921 \pm 0.050$ ;  $D(\mathcal{C}_1) = 0.049 \pm 0.028$ ;  $D(\mathcal{C}_2) = 0.049 \pm 0.020$ ;  $D(\mathcal{C}_1, \mathcal{C}_2) = 0.162 \pm 0.135$ . The results clearly show that the hierarchical structure is real, and not a mere artifact of Ward's algorithm.

A striking demonstration of this point can be seen in Fig. 2(b), which shows the distance matrix  $D_{\mu\nu}$  between the GS that were ordered in Fig. 2(a). Dark represents short distances and light - high. If we cluster states with  $S_i = \pm 1$  at random, the reordered distance matrix is a greyish square. Only when the clustered states form a real, well defined hierarchy, does the reordered distance matrix reveal the structure so clearly seen in Fig. 2(b). To understand this hierarchy of GS we investigated the organization of the  $N$  spins in the  $M$  GS.

*Clustering the spins:* We cluster  $i = 1, \dots, N$  spin-vectors  $\mathbf{S}_i = (S_i^1, S_i^2, \dots, S_i^M)$ , looking for correlated spin domains. Define a distance between spins  $i$  and  $j$  by  $d_{ij} = 1 - c_{ij}^2$ , where  $c_{ij} = \mathbf{S}_i \cdot \mathbf{S}_j / M$  is the correlation between spins  $i$  and  $j$ . Note that  $c_{ij}^2$  is the relevant measure of correlations in a spin glass. A typical outcome of clustering the spins with this distance matrix is the dendrogram  $\mathcal{D}$  of Fig. 3(a), obtained for the same system, whose GS were studied in Fig. 2. In Fig. 3(b) we show the distance matrix obtained *after* the spins have been reordered according to  $\mathcal{D}$ . Non-trivial structure in spin space is evident; dark squares along the diagonal represent highly correlated clusters.

*Identifying  $\mathcal{G}_1$  and  $\mathcal{G}_2$ .* In order to identify  $\mathcal{G}_1$ , the

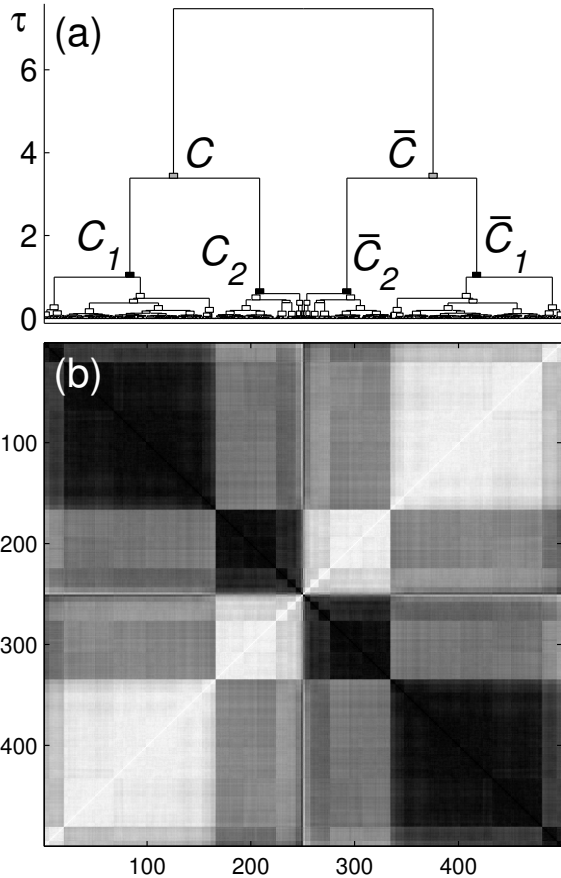


FIG. 2. (a) The dendrogram obtained by clustering the ground states, for a particular set of  $J_{ij}$ , for  $N = 6^3$  spins. (b) When the states are ordered according to the dendrogram, a clear block structure is seen in  $D_{\mu\nu}$ , the distance matrix of the GS. Darker shades correspond to shorter distances.

largest domain of correlated spins, we go over all pairs of GS,  $\mu, \nu$ , with  $\mu \in \mathcal{C}$  and  $\nu \in \bar{\mathcal{C}}$ , and identify  $\mathcal{G}_{\mu\nu}$ , the set of spins that have opposite signs in  $\mu$  and  $\nu$ . For all  $L$  and  $\{J\}$ , the set  $\mathcal{G}_{\mu\nu}$  is contiguous for more than 99.5% of the pairs. Thus,  $\mathcal{G}_{\mu\nu}$  can be related to the low energy droplet excitations found for SRSF with Gaussian couplings [5,15].

For a given  $\{J\}$  we identify as  $\mathcal{G}_1$  the largest contiguous group of spins shared by at least a fraction  $\theta = 0.95$  of the sets  $\mathcal{G}_{\mu\nu}$ . Thus, inside  $\mathcal{G}_1$   $c_{ij}^2 \geq 0.81$  (for  $L = 8$  the average correlation inside  $\mathcal{G}_1$  is always larger 0.94). The second largest spin domain,  $\mathcal{G}_2$ , is found in a similar way, by scanning all pairs of GS with  $\mu \in \mathcal{C}_1$  and  $\nu \in \mathcal{C}_2$ . As seen in Fig. 4, the average sizes of  $\mathcal{G}_1, \mathcal{G}_2$  do not change a lot for  $0.60 < \theta < 0.95$ .

According to our picture we expect  $|\mathcal{G}_a| \propto L^d$  for both  $a = 1, 2$ . We present the distributions of  $|\mathcal{G}_a|/L^3$  for  $4 \leq L \leq 8$  in Fig. 5. Our results show that the sizes of the two largest spin clusters do scale as  $L^3$ .

We turn now to identify those clusters  $g_1, g_2$  in our spin dendrogram, which can be associated most naturally

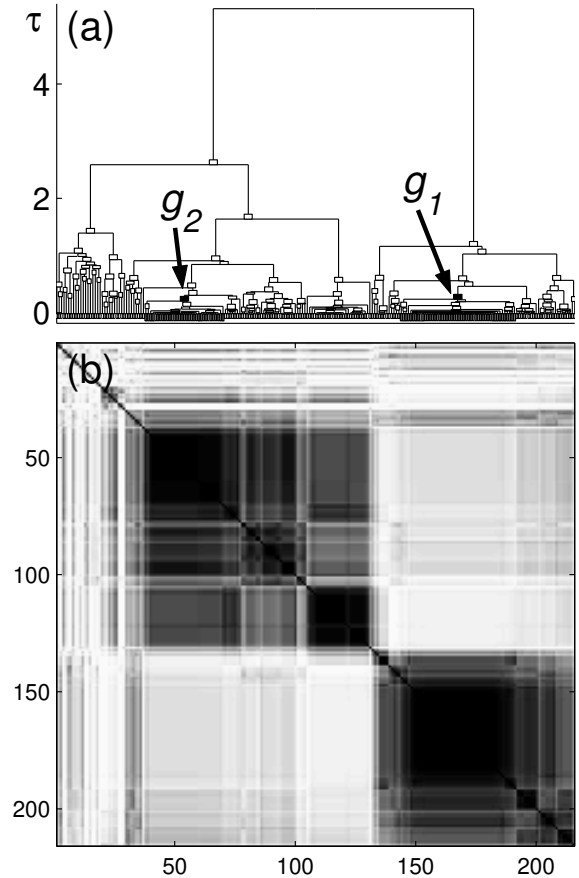


FIG. 3. (a) The dendrogram  $\mathcal{D}$  obtained by clustering the spins of the system of Fig. 2. For this realization  $g_a = \mathcal{G}_a$  for both  $a = 1, 2$ . (b) When the spins are ordered according to the dendrogram, a structure of correlated spin domains emerges; darker shades correspond to shorter distances and higher correlations.

with the domains  $\mathcal{G}_1, \mathcal{G}_2$ .  $g_1$  is that cluster which is most similar to  $\mathcal{G}_1$ , i.e. has the largest fraction of shared spins  $\mathcal{S}(g_1, \mathcal{G}_1) = 2|g_1 \cap \mathcal{G}_1|/(|g_1| + |\mathcal{G}_1|)$ . The similarity is high: for  $L = 8$  on the average we have  $\mathcal{S}(g_a, \mathcal{G}_a) = 0.99(1)$  for  $a = 1$  and  $0.97(4)$  for  $a = 2$ . This means that  $\mathcal{G}_1$  and  $\mathcal{G}_2$  do have a meaningful role in spin space, and are not just an artifact of our analysis.

*Overlap distribution:* Our picture yields a non-trivial overlap distribution  $P(q)$  [5–7,15]. Having identified GS clusters, we can decompose  $P(q)$  into its main components and elucidate the physics underlying its structure. For example, we present in Fig. 6, for a single realization, the distribution  $P_{\mathcal{C}\bar{\mathcal{C}}}(q)$  of overlaps  $q_{\mu\nu}$  between pairs of GS  $\mu \in \mathcal{C}$  and  $\nu \in \bar{\mathcal{C}}$ . Typically  $P_{\mathcal{C}\bar{\mathcal{C}}}(q)$  is dominated by two large peaks, centered at  $q_1$  and  $q_2$ , as in Fig. 6.

The overlap  $q_{\mu\nu}$  is directly related to the size of the set  $\mathcal{G}_{\mu\nu}$  of flipping spins:  $|\mathcal{G}_{\mu\nu}| = (1 - q_{\mu\nu})N/2$ . By our definition of  $\mathcal{G}_1$ , in general  $\mathcal{G}_1 \subset \mathcal{G}_{\mu\nu}$ . A large part of the sets  $\mathcal{G}_{\mu\nu}$  also include  $\mathcal{G}_2$ . This part will contribute to the peak at  $q_2$ , so  $(1 - q_2)N/2 > |\mathcal{G}_1 \cup \mathcal{G}_2|$ . The others, which

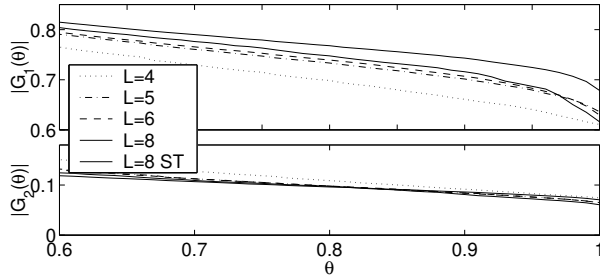


FIG. 4. The average sizes of  $\mathcal{G}_1(\theta)$  and  $\mathcal{G}_2(\theta)$ . The thin solid line presents only ST data for  $L = 8$ , which are unbiased but highly noisy due to the relatively small number of (60) realizations.

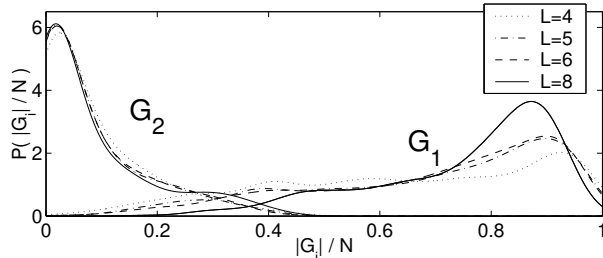


FIG. 5. Size distribution of  $\mathcal{G}_1$  and  $\mathcal{G}_2$ . Note that the distribution of  $\mathcal{G}_2$  seems to converge already for  $L = 8$ . The distribution of  $\mathcal{G}_1$  converges for sizes between  $0.5N$  and  $0.7N$ .

do not include any part of  $\mathcal{G}_2$ , will contribute to the peak at  $q_1$ , so  $N - |\mathcal{G}_2| > (1 - q_1)N/2 > |\mathcal{G}_1|$ . We confirmed these predictions by measuring three quantities:  $r_1 = (1 - q_1)N/2|\mathcal{G}_1|$ ;  $r_2 = (1 - q_2)N/2|\mathcal{G}_1 \cup \mathcal{G}_2|$ ;  $r_3 = (1 - q_1)N/2(N - |\mathcal{G}_2|)$ .  $r_2$  and  $r_3$  were measured and averaged only over realizations with non-vanishing  $\mathcal{G}_2$  (79% of the realizations for  $L = 6$  and 80% for  $L = 8$ ). The results for  $L = 6$  were  $r_1 = 1.39(\text{mean}) \pm 0.61(\text{s.d.})$ ;  $r_2 = 1.23 \pm 0.27$ ;  $r_3 = 0.89 \pm 0.15$ ; and for  $L = 8$ :  $r_1 = 1.21 \pm 0.25$ ;  $r_2 = 1.19 \pm 0.16$ ;  $r_3 = 0.92 \pm 0.12$ .

Our picture yields a non-trivial  $P(q)$ , as indeed we found in all systems examined (e.g. Fig. 6). On the other hand, works by one of us [19] and others [20], predicted trivial  $P(q)$  at zero and finite  $T$ . This may suggest that the findings described above are the result of finite size effects and that  $P(q)$  is trivial at  $L = \infty$ .

Fig. 5 strongly suggest that  $\mathcal{G}_2$  does *not* vanish as  $L$  increases, and thus the two peaks of  $P(q)$  will remain separated. Still, the distribution may become trivial if

$$\bar{c}_{12} = \frac{1}{|\mathcal{G}_1||\mathcal{G}_2|} \sum_{i \in \mathcal{G}_1} \sum_{j \in \mathcal{G}_2} c_{ij}^2 \rightarrow 1 \quad \text{as } L \rightarrow \infty \quad (4)$$

In this case  $\mathcal{G}_1$  and  $\mathcal{G}_2$  will always flip together, and the peak at  $q_1$  will vanish. We carried out fits of the form  $\bar{c}_{12}(L) = \bar{c}_{12}(\infty) - AL^{-\phi}$  with  $A$  and  $\phi$  as fit parameters. The minimum of  $\chi^2$  is  $1.7 \times 10^{-4}$  for  $\bar{c}_{12}(\infty) = 0.54$ . For  $\bar{c}_{12}(\infty) = 1$  we have  $\chi^2 = 3.4 \times 10^{-4}$ . Our result  $\bar{c}_{12}(\infty) < 1$  should be tested further for larger systems.

*Summary:* The ground states of the  $\pm J$  short-range

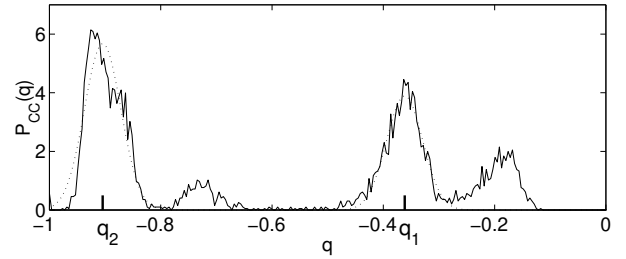


FIG. 6. The distribution  $P_{cc}(q)$  for a single system of size  $8^3$ . The peak positions at  $q_1$  and  $q_2$  are determined by a fit to the sum of two Gaussians (dotted line). The two smaller peaks are probably due to a third correlated spin domain  $\mathcal{G}_3$ .

Ising spin glass have a hierarchical, tree-like structure. This structure is induced by correlated spin domains, which are the cores of macroscopic zero energy excitations, taking the system from one state-cluster to another. This structure of GS and the associated barriers has some features of the RSB based picture, but is inconsistent with it. It is, however, consistent with the droplet picture.

We thank the Germany-Israel Science Foundation for support, I. Kanter and M. Mezard for helpful discussions, and N. Jan for hospitality to DS.

- 
- [1] M. Mézard, G. Parisi, N. Sourlas, G. Toulouse and M. A. Virasoro, J. Phys. **45**, 843 (1984).
  - [2] D. Sherrington and S. Kirkpatrick, Phys. Rev. Lett. **35**, 1792 (1975).
  - [3] E. Marinari, G. Parisi and J. J. Ruiz-Lorenzo, Phys. Rev. B, **58**, 852 (1998).
  - [4] D. S. Fisher and D. A. Huse, Phys. Rev. B **38**, 386 (1988).
  - [5] F. Krzakala and O. C. Martin, Phys. Rev. Lett. **85**, 3013 (2000).
  - [6] H. G. Katzgraber, M. Palassini, A. P. Young, cond-mat/0007113 (2000).
  - [7] S. Franz and G. Parisi, cond-mat/0006188 (2000).
  - [8] D. A. Huse and D. S. Fisher, J. Phys A **20**, L997 (1987).
  - [9] S. F. Edwards and P. W. Anderson, J. Phys. **F5**, 965 (1975).
  - [10] In fact we ensured to have equal numbers of positive and negative bonds.
  - [11] S. Kirkpatrick, Phys. Rev. B **16**, 4630 (1977).
  - [12] A. K. Hartmann, Physica A **224**, 480 (1996); Phys. Rev. E **59**, 84 (1999).
  - [13] W. Kerler and P. Rehberg, Phys. Rev. E **50**, 4220 (1994).
  - [14] F. Barahona, R. Maynard, R. Rammal and J. P. Uhty, J. Phys A **15**, 673 (1982).
  - [15] M. Palassini and A. P. Young, Phys. Rev. Lett. **85**, 3017 (2000)
  - [16] A. W. Sandvik, Europhys. Lett. **45**, 745 (1999).
  - [17] A. K. Hartmann, J. Phys. A **33**, 657 (2000).
  - [18] A. K. Jain and R. C. Dubes, *Algorithms for Clustering Data*, Prentice-Hall, Englewood Cliffs (1988).
  - [19] A. K. Hartmann, Eur. Phys. J. B **13**, 539 (2000).
  - [20] N. Hatano and J. E. Gubernatis, cond-mat/0008115 (2000); see, however, E. Marinari, G. Parisi, F. Ricci-Tersenghi and F. Zuliani, cond-mat/0011039 (2000).